COMPUTATIONAL ASSESSMENT OF THE STRUCTURAL PERFORMANCE OF CONCRETE BEAMS WITH ENCASED STEEL JOIST

R. BALLARINI[1], L. LA MENDOLA[2], J. LE[3], AND A. MONACO*[4]

[1] Dept. of Civil and Environmental Engineering, Cullen College of Engineering, Univ. of Houston
N127 Engineering Bldg. 1, Houston, TX 77204-4003
rballarini@uh.edu

[2] Dept. of Civil, Environmental, Aerospace and Material Engineering, Univ. of Palermo
Viale delle Scienze Edificio 8, 90128 Palermo, Italy
lidia.lamendola@unipa.it

[3] Dept. of Civil, Environmental, and Geo-Engineering, Univ. of Minnesota
500 Pillsbury Dr. SE, Minneapolis, MN 55455-0116
jle@umn.edu

[4*] Dept. of Civil, Environmental, Aerospace and Material Engineering, Univ. of Palermo
Viale delle Scienze Edificio 8, 90128 Palermo, Italy
alessia.monaco@unipa.it

Key words: FEM modelling, Fracture, Size and geometrical effects, Composite structures.

Abstract. This study concerns the computational assessment of the failure modes of hybrid beams made up of prefabricated steel truss encased within a concrete block and named hybrid steel trussed concrete beams (HSTCBs). The considered failure mode is under three-point bending and the adopted approach is developed by means of finite-element (FE) simulations of beams of different scaled sizes, whose design corresponds to current industrial practice. The FE model is based on well-established constitutive relations of both concrete and steel. In particular it employs a continuum damage model for concrete (concrete damaged plasticity model) and a classical elastic-plastic multi-linear behavior for steel. As regards contact at the interface, two different approaches are used and compared: a simplified contact condition able to simulate perfect bond and a non-linear cohesive interaction capable of reproducing the progressive degradation of the initial contact condition. Furthermore, models are generated also employing finite elements of different type and order and, therefore, the computational efforts required by each model are compared in order to evaluate the efficacy of the simplest modelling type able to retain the salient features of the structural mechanism. Existing experimental data are used for validating the numerical results. The simulations on specimens of three different sizes show that, in the absence of three-dimensional geometrical similarity, the small-size beam exhibits shear failure while the large-size beams attain a more ductile failure under flexure. The numerical results allow observing a transition between different failure modes, which indicates the importance of employing a robust three-dimensional FE model for design extrapolation of HSTCBs across different sizes and geometries.

1 INTRODUCTION

The Hybrid Steel Trussed Concrete Beams (HSTCBs) represent a commonly used structural solution for beams in seismic areas for both framed civil structures and light industry buildings. This type of beam is usually constituted by a prefabricated steel joist made up of ribbed or smooth steel bars embedded into a cast-in-place concrete core, as shown in Figure 1. HSTCBs are especially employed in the Italian construction industry since almost fifty years thanks to the numerous advantages of their use. In fact, they allow significant reduction of the construction time thanks to the partial prefabrication; moreover no formwork are required due to the presence of the bottom steel plate, which is part of the prefabricated steel joist; in situ welding or tying are not required and risk of injury is minimized because no intermediate supports are required when specific end-devices are employed at beam-to-column joints (Figure 1). Finally, HSTCBs are able to cover large spans with relatively small beam depths.

In the last decades, several researches have been carried out on the behavior of HSTCBs. Among others, the main investigated issues were the flexural and shear strengths of the beam [1-6], the behavior of beam-to-column joints and connections [4,7], the stress transfer from the bottom chord of the truss to the concrete core [5,8-10]. All researches highlighted that the complex three-dimensional (3D) geometry of the beam and the nonlinear constitutive behaviors of the materials make it difficult to develop a single analytical model for predicting the failure load of HSTCBs. Moreover, most studies deal with slab-thick beams and do not take into account the effects of different sizes on the mechanical response of HSTCBs. This fact is also due to the difficulty of testing large-scale specimens in laboratory and then interpreting the experimental results and deriving design formula. For this reason, the development of computational models through finite element method (FEM) becomes an essential research tool. This is what motivates the present work.

This paper presents a numerical study of the failure behavior of HSTCBs of different sizes, including large-scale specimens. The influence of specimen size and geometry on the structural failure has been observed and studied by several researchers with regard to structures made of many types of concrete materials [11-13]; in this frame, the authors recently proposed a first computational study on the structural failure of HSTCBs [14].

The understanding of the size and geometrical effects could lead to the improved design procedure since many full-scale designs have to rely on the extrapolation of laboratory experiments on small-scale specimens. Meanwhile, the analysis of the size and geometrical effects has also inspired advanced analysis techniques for both classical and new problems [15,16].

In this work, FEM models are generated also employing finite elements of different type and order and, therefore, the computational efforts required by each model are compared in order to evaluate the efficacy of the simplest modelling type able to retain the salient features of the structural mechanism. Existing experimental data and numerical benchmark are used for validating the results. Finally, the observed overall size and geometrical effects on the peak load capacity of HSTCBs are discussed.
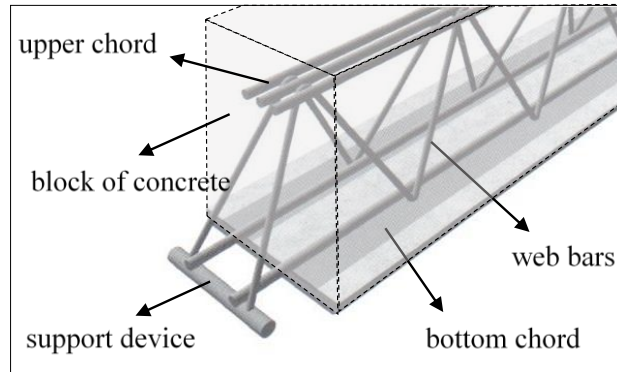
Figure 1: Topology of HSTCB (redrawn from Ref. [14])

2 FINITE ELEMENT MODEL GENERATION

The numerical model is developed with the aim of retaining the salient features of the mechanical response of the HSTCB, on one side, and computational efficiency for the design purpose, on the other side.

For these reasons, the steel reinforcement constituted by both rebars and bottom plate is modeled using beam and shell elements, respectively, while concrete is modeled using first order tetrahedral finite elements. A preliminary convergence study allowed determining the most suitable mesh size.

Regarding materials, the constitutive behavior of concrete is modeled by means of a continuum damage plasticity model [17], which combines the theory of continuum damage mechanics and the theory of plasticity. Moreover, the crack band model is used [18] in order to mitigate spurious mesh dependency of FE simulation of concrete fracture due to its strain softening behavior. The fracture energy G_f represents the input parameter in the definition of the tensile behavior of concrete and as a consequence the tensile stress-strain curve is adjusted as a function of element size in order to preserve the constancy of the fracture energy.

The constitutive relationship of steel is assumed to follow a metal plasticity model with elasto-plastic hardening behavior. In this model, the von Mises yield surface with an isotropic hardening rule is used to describe the plastic flow, in which the yield surface changes its size uniformly in all plastic strain directions.

As simplified hypothesis, the steel bars are assumed perfectly bonded to the concrete material so that the modeling of the highly non-linear interface behavior is not required. This simplified assumption will be validated by comparing the results of such a model with those of a more complex model in which the interface behavior is implemented by using a non-linear cohesive interaction between surfaces.

FEM simulations of three-point bending tests on HSTCBs of three sizes were performed using the general purpose FE analysis software ABAQUS 6.12 [19] for investigating the influence of size and geometry on the failure behavior of such beams. The three different sizes of beams are here denoted as specimens S1, S2 and S3; their geometry is reported in Figure 2. The span-to-depth ratio of specimen S1 is $a/D = 2.4$; this value is kept the same also for the other two specimens. The depths of the beams are chosen so that specimens S1, S2 and S3 have a size ratio 1: 2.22: 4.93. The width b is kept constant, equal to 300 mm. The size of the steel reinforcement (rebars and bottom plate) is kept constant according to the most

adopted industrial practice, while the horizontal span of the diagonal steel truss is linearly scaled with the beam depth. It is noteworthy to remark that specimens S1 and S2 represent typical sizes that can be used in practice. Consequently, the cross sections of the specimens present an increasing slope of the diagonal rebars, which results equal to 68°, 81° and 86° for specimens S1, S2 and S3, respectively.

Therefore, it has to be stressed that, based on these assumptions, the examined specimens do not exhibit geometrical similarity, fact that has a profound implication on the failure behavior of the beams. Finally, all specimens are considered to be made of the same type of materials, i.e. concrete with compressive strength of 25 MPa, class B450C steel for the longitudinal and diagonal rebars and class S355 steel for the bottom plate.
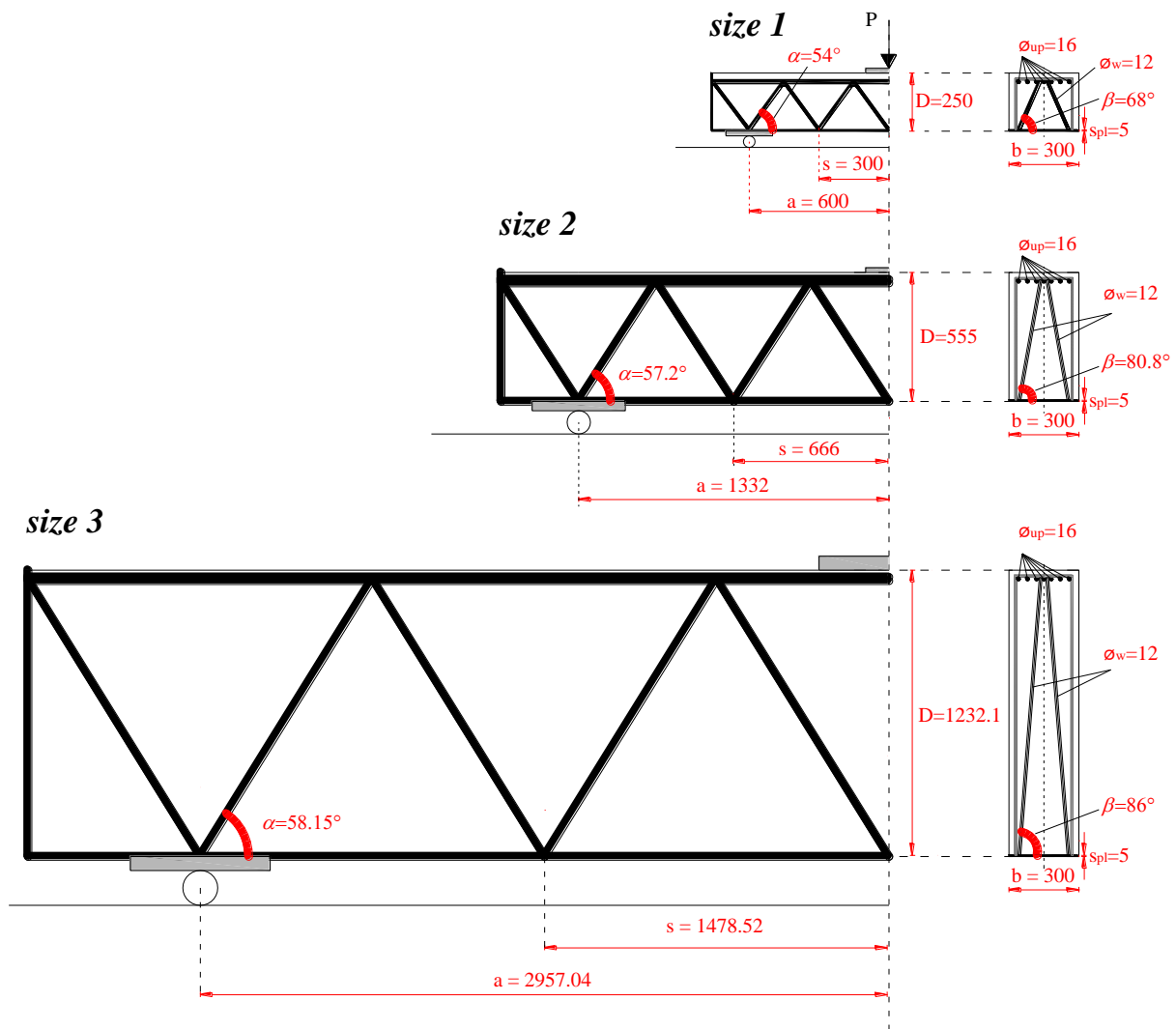
Figure 2: FEM model features (dimensions in mm) (redrawn from Ref. [14])

3 EXPERIMENTAL AND NUMERICAL BENCHMARK FOR VALIDATION

In order to validate the proposed FEM model, two benchmarks are used: the experimental results of recent three-point bending tests conducted on specimen S1 [5] and the outputs of a different FE simulation in which a more realistic cohesive law for the steel-concrete interface is used in the modeling of all beam sizes [6,14]. These comparisons will allow validating the suitability of the simplified assumption of the perfect bonding of the steel-concrete interface for the purpose of the prediction of the load capacity of HSTCBs by means of robust and computationally efficient FE model.

Experimental tests of three-point bending have been performed on specimen S1 at the University of Palermo [5]. The cross-section of the specimen has a dimension of 250 mm depth and 300 mm width; the prefabricated steel truss is made up of 16 mm-diameter rebars on the top, 5 mm-thick steel plate at the bottom and 12 mm-diameter diagonal rebars. The rebars are made of ribbed steel with yielding strength $f_y = 450$ MPa while the lower plate is made of smooth steel with $f_y = 355$ MPa. The design compressive strength of concrete f_c is 25 MPa. The shear span a is equal to 600 mm and the bottom steel plate is anchored at the ends of the beam in order to avoid slip between the plate and the concrete.

Two specimens of type S1 were tested, denoted as specimen A1-1 and A1-2, respectively. These tests were performed in displacement control, monitoring the mid-span deflection by external LVDTs, while the strains of the steel bars and the bottom plates were measured by electrical strain gauges.

Analyzing the test results reported in Figure 3, it is possible to observe how flexural cracks start to develop at the bottom of the specimen as the load reaches about 120 kN, afterwards, for increasing load values, diagonal shear cracks start to initiate and propagate while the growth of the aforementioned flexural cracks becomes insignificant [5]. When the beam reaches its peak strength, significant diagonal shear cracking is observed, which leads to the subsequent loss of load capacity. Finally, the embedded ductile steel trusses allow retaining a residual load capacity of about 200 kN for large displacements.

Figure 3 also presents the comparison between the experimental load-displacement curves of S1 specimen and those simulated by the FE model. The simulated curve is denoted as "Model 1 (perfect bond)" in the figure. It is evident that the present model overestimates the initial stiffness of the beam due to the hypothesis of perfect bond at the steel-concrete interface. Concerning the global mechanism, the FE simulation shows that the beam exhibits an overall brittle failure with sudden drop of the load-carrying capacity right after the peak load. Subsequently, the beam exhibits a residual load-carrying capacity in accordance with the experimental tests. FE outputs allow observing that, at the initial loading phase, the concrete experiences flexural damage at the bottom of the beam followed by the yielding of the steel truss and plate. The flexural failure of concrete does not lead to a significant loss of load capacity since the tensile stress generated by the bending is primarily taken by the steel elements and, in particular, by the bottom plate. Therefore, the flexural damage that affects the tensile concrete in this stage does not contribute to the failure of the beam. Conversely, when the peak strength is attained, extensive compressive failure occurs almost along the direction of the compressed diagonal steel bars in the form of a narrow band. This indicates that a compression strut is formed along the diagonal direction, which starts to experience damage signifying the diagonal shear failure.

5

With the aim of further investigating the role of steel-concrete interface, the three-point bending test of specimen S1 is simulated also by considering a nonlinear model for the interfacial behavior [6,14]. In such a model, the interfacial slip is determined as $\delta = \sqrt{\delta_s^2 + \delta_t^2}$, where δ_s and δ_t are the slips along the two orthogonal directions in the plane of the interface. The work-conjugate effective shear traction needs to satisfy the relationship:

$$\tau \, \mathrm{d}\delta = t_s \, \mathrm{d}\delta_s + t_t \, \mathrm{d}\delta_t \tag{1}$$

where t_s and t_t are the shear tractions in the two orthogonal directions in the plane of the interface. Eq. 1 has to be satisfied for any values of $\mathrm{d}\delta_s$ and $\mathrm{d}\delta_t$. This condition yields $t_s = \tau \delta_s / \delta$ and $t_t = \tau \delta_t / \delta$. Therefore, the behavior of the steel-concrete interface can be described by the relationship between the net slip and the effective shear traction.

Figure 3 shows the load-deflection curve simulated by such a detailed FEM model with non-linear interfacial behavior, together with that simulated by the proposed simplified model and the experimental measurement. It is seen that the result of the benchmark detailed model agrees well with the experimental result. On the other hand, the comparison with the simulation performed by using the simplified model shows that the use of a more realistic steel-concrete interfacial behavior would allow catching better the overall beam stiffness. However, the detailed modeling of the non-linear interface does not significantly affect the peak load as well as the total energy dissipation. This is because the steel-concrete interface does not experience significant damage in the meaning that, as expected, the energy dissipation along the interface is small compared to the dissipation due to concrete damage and steel plasticity. Therefore, the simplified model proves to be sufficient for modeling the failure behavior of specimen S1 and requires a more contained computational time. The comparison between the present model and the chosen benchmark shows that the present model can well capture various essential failure mechanisms as well as the peak load capacity of the beam even though it does not predict well the initial elastic stiffness of the beam.
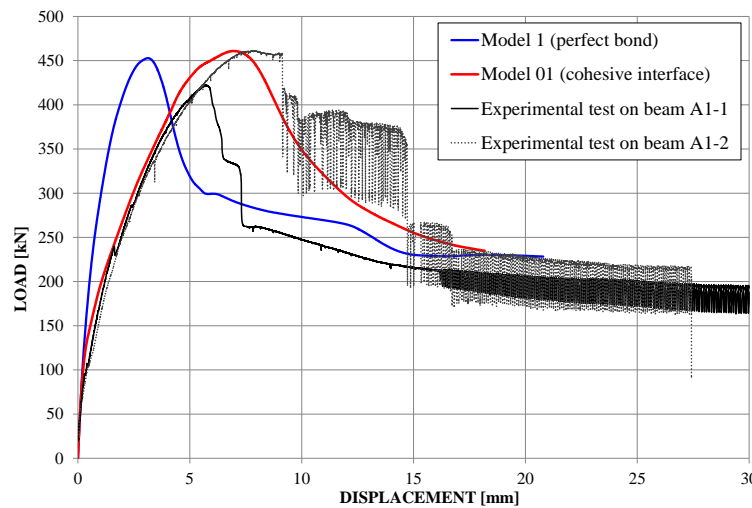

Figure 3: Comparison between detailed and simplified FEM models against the experimental results

4   RESULTS OF FINITE ELEMENT SIMULATIONS

Based on the FE model description and validation, the simulation of the failure behavior of specimens S2 and S3 is now performed assuming the perfect bond model, which is able to provide a reasonable prediction of failure mechanisms of specimens because the damage of the steel-concrete interface has an insignificant effect on the overall failure behavior. Moreover, for validation, the benchmark detailed FE model is used to simulate the behavior of specimens S2 and S3.

Figure 4 shows the numerical load-deflection curves of specimens S2 and S3 by using the present model (Model 2/3 perfect bond) and the benchmark model (Model 2/3 cohesive interface). It is seen that the curves are very similar for both specimens. It is noteworthy to observe that for these large scale specimens there is no significant difference in the initial slope of the simulated curves, as instead observed for specimen S1.This is attributable to a less influence of the initial elastic response of the steel-concrete interface on the elastic response of specimens S2 and S3. In this regard, it has to be reminded that the dimension of the steel truss is not scaled proportionally with the concrete beam size.

Figure 4 indicates that, differently from specimen S1, specimen S2 exhibits a prevalently ductile behavior with almost constant load value for a large range of displacements before the ultimate loss of load capacity. During the initial loading phase, concrete damage occurs in the mid-span of the beam mainly due to the bottom steel plate, which is pulled upward by the two diagonal truss bars (Figure 5a), inducing local compression on concrete. When the specimen achieves the peak load, the bottom plate and the diagonal rebars of the truss have already yielded and diffused flexural cracks can be observed in the concrete (Figure 5b). In the diagonal direction, the compressive strength of concrete is reached. It is also possible to observe limited compressive failure in the mid-span of the beam where the local deformation of the bottom plate induces local compressions.

For specimen S2, the overall damage is concentrated mainly along the diagonal directions while it is more limited in the mid-span of the beam. This fact is very different from the failure mechanism observed in specimen S1, in which cracking is concentrated along the diagonal directions. For this reason, the beam exhibits an overall ductile behavior, the diagonal compressive damage being limited. Furthermore, the fact that the steel truss has a steeper angle in the transversal direction, induces a confinement effect of the concrete material that suppresses the diagonal shear cracking. In addition, other factors, such as the aspect ratio of the cross section, may also influence the failure mode of the beam. A detailed parametric study is suitable for investigating the effects of these factors.

The simulation showed that the dominant failure mode of specimen S2 is not diagonal shear failure as in specimen S1, therefore it is expected that the interfacial damage in this specimen would be less than that of specimen S1. The post-peak regime of the load-deflection curve allows confirming this consideration: in fact, the curve simulated by the perfect bond model is almost close to that simulated by the model with non-linear interfacial behavior.

With regard to specimen S3, it can be noted that diffused cracks appears at the bottom of the beam in the initial loading steps. Subsequently, compressive damage also appears along the diagonal directions. However, at the peak load, the predominant failure mechanism is characterized by flexural damage at the mid-span of the beam. After the peak, the maximum plastic principal strains continuously increase in the diagonal directions. It is noteworthy to

mention that the width of the cracks in the diagonal direction tends to increase and become comparable to the flexural cracks. This is the predominant cracking pattern observed in the simulation, which proves to remain almost the same till the end of the analysis (Figure 6).

The comparison between the failure modes of specimens S2 and S3, shows that specimen S3 exhibits less ductility. In particular, even though the diagonals of the steel truss in S3 have a steeper angle in the transverse direction, it is noted that, in the longitudinal direction, the amount of concrete between the steel trusses in specimen S3 is larger than that in specimen S2. Consequently, the confinement effect previously seen for specimen S2, would be less significant in specimen S3. On the other hand, if compared to the failure behavior of specimen S1, specimen S3 exhibits a more ductile response, which indicates that the confinement effect in the large specimen is more pronounced than in the smaller one. Specimen S3 exhibits a combined flexural and shear damage in the post-peak regime; this fact also explains the difference in the post-peak curves simulated by the present model and the benchmark model, which becomes more pronounced as compared to specimen S2 where only the flexural damage is dominant the post-peak regime.
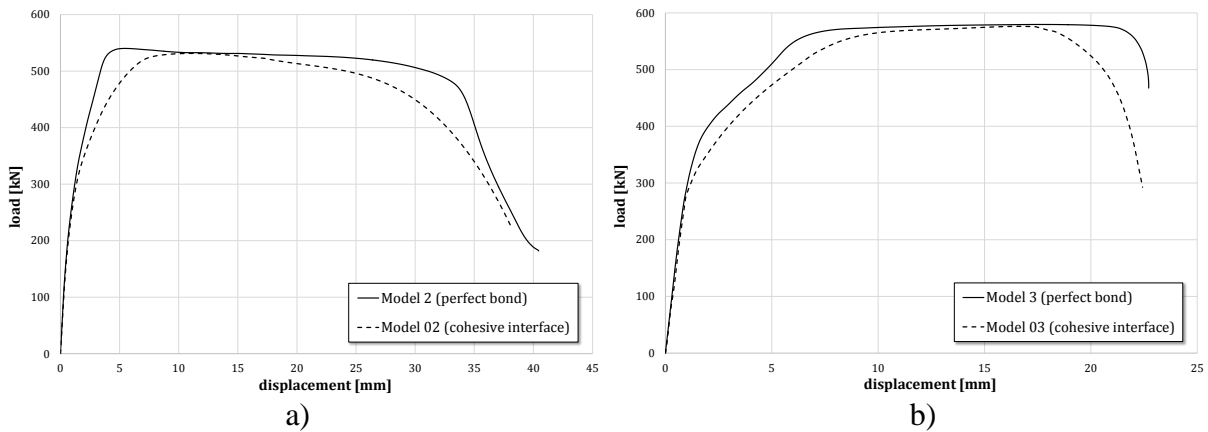

Figure 4: Simulated load-dflection curves for: a) specimen S2 and b) specimen S3 [14]
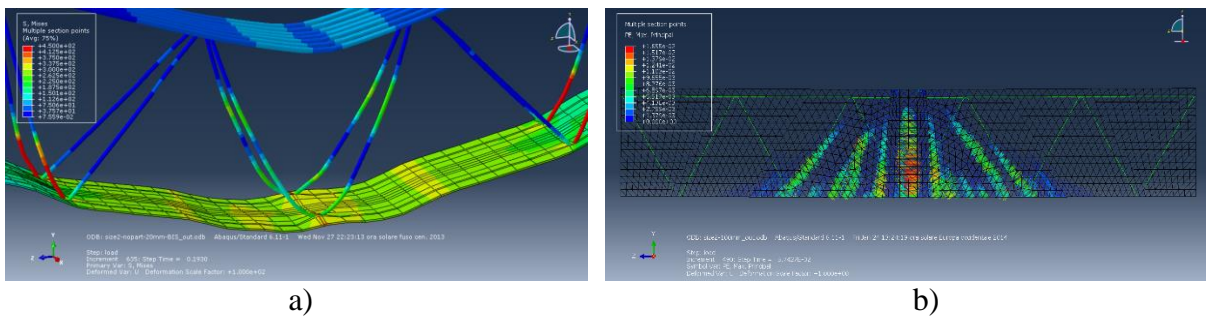

Figure 5: Damage mechanism of specimen S2: a) local deformation of the truss; b) maximum strain profile
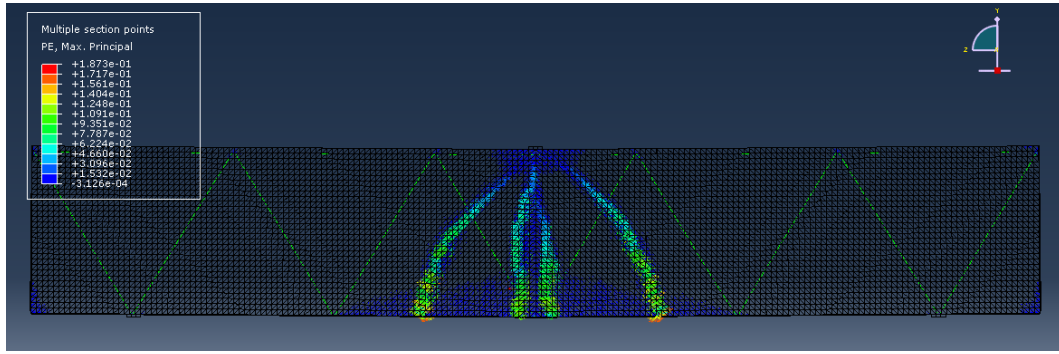
8

Figure 6: Cracking patterns of specimen S3 at the ultimate failure

5   DISCUSSION ON FAILURE MODES

As discussed above, the FE simulations showed two principal failure behavior in concrete, i.e. flexural failure at the mid-span and shear failure in the diagonal direction.

With regard to the first mode, flexural failure of HSTCBs can be depicted as a ductile mode in which the load is carried essentially by the bottom steel plate while tensile concrete is cracked. Conversely, the second failure mode is typically quasibrittle and causes a sudden loss of load-carrying capacity after the peak strength is reached.

 FE simulations showed the influence of the three-dimensional complex geometry of the HSTCB in the relative dominance of these two failure modes, because the arrangement of the steel truss theoretically induces different confinement levels on concrete and allows delaying or accelerating the diagonal shear crisis.

It is well known that, in classical reinforced concrete (RC) beams, analytical scaling models for the evaluation of the size effect in the load-carrying capacity are available for geometrically similar specimens with the same failure mode (e.g. [20-22]). Conversely, the three specimens examined in this study do not follow geometrical similarity and, therefore, the size and geometrical effects on the peak load can be explained qualitatively without applying rigorously the existing analytical scaling models.

Generally, for analyzing the size effect, the nominal structural strength σ_N is used as a load parameter. This stress is thus defined as:

$$\sigma_N = P_{\max} / bD \tag{2}$$

in which P_{max} is the maximum load capacity and the dimensions D and b are the beam depth and width, respectively.

It has been seen that the predominant failure mode of specimen S1 is the diagonal shear failure. Such a failure mode has been extensively investigated for analyzing the size effect of RC beams and the equation proposed for the variation of the nominal strength is [20,22]:

$$\sigma_N = \sigma_0 \left(1 + D / D_0\right)^{-1/2} \tag{3}$$

In Eq. 3 σ_0 is the nominal structural strength at the small-size limit while D_0 represents the transitional size. Both σ_0 and D_0 depend on the structural geometry, material strength and fracture properties. In particular, Eq. 3 is used for defining the transition from quasi-plastic shear failure to brittle shear failure as the specimen size becomes much larger than the size of

the fracture process zone.

It can be observed that the shear failure experienced by HSTCBs basically retains the same mechanism as the diagonal shear failure of conventional RC beams. Consequently, Eq. 3 can be considered an adequate approximation of the size effect in shear failure of HSTCBs.

On the contrary, specimens S2 and S3 experienced a significant flexural damage with more limited diagonal shear failure after the peak load. Therefore, neglecting the damage of concrete in the diagonal direction and assuming that tractions on the bottom of the beam are taken by the yielded steel plate, then the ultimate bending moment M_u can be simply calculated as $M_u = F_y A_s \bar{d}$, where F_y is the yielding strength of steel, A_s is the area of the steel plate and $\bar{d}$ is the effective depth of the beam. Consequently, the maximum load P_u of the beam subjected to three-point loading is equal to $P_u = 4 F_y A_s \bar{d} / L$. In the latter expression, the ratio $\bar{d} / L$ can be taken as a constant, the dimension of the beam being geometrically scaled in 2D. Under this assumptions, the load capacity of the HSTCB would be independent of the beam size and, therefore, the corresponding scaling equation for σ_N can be written as

$$\sigma_N = \eta D^{-1} \tag{4}$$

where $\eta = 4 F_y A_s \bar{d} / bL$.

In Figure 7 the relationship between the nominal strengths of specimens S1-S3 and their sizes are plotted on the log-log scale, together with Eqs. 3 and 4. In particular, the figure shows only a schematic plot of Eq. 3 because σ_0 and D_0 cannot be determined based on only one simulation point for the diagonal shear failure mode. The plot shows that for specimens S2 and S3 the simulated size effect is consistent with Eq. 4. while, for specimen S1, it is expected to follow Eq. 3.

Based on the aforementioned analysis, the nominal strength of the beam can be understood as the minimum value of the nominal strengths predicted by Eqs. 3 and 4:

$$\sigma_N = \min\left[\eta D^{-1}, \sigma_0 \left(1 + D / D_0\right)^{-1/2} \right] \tag{5}$$

Furthermore, Figure 7 also shows that there is a transition between these two size effects, which depends on both the size and geometry of the HSTCB. However, in this type of beam, the complex geometry of the steel joist and the confinement effect induced in the concrete material, make it difficult to derive a simple analytical solution for the nominal strength able to take into account both failure modes.

Finally, it is noteworthy to observe that Eq. 5 predicts a size effect with $\sigma_N \propto D^{-1}$ for flexural failure. This is due to the fact that in the examined specimens the bottom steel plate is not scaled proportionally with the beam size, conversely, a 5-mm thick plate is adopted in all specimens, in accordance with the current industrial practice.

It is clear that this assumption greatly penalizes the nominal strength for large-size beams. If the steel plate thickness were proportionally scaled with the beam size, the size effect on nominal strength for the flexural failure mode would vanish. As a result, only the diagonal shear failure mode would be observed, which could be subjected to a strong size effect in the absence of shear stirrups [15,16].
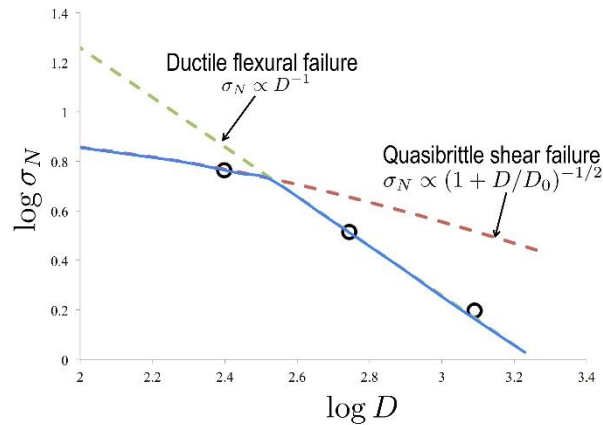
Figure 7: Simulated size effect on the nominal structural strength (redrawn from Ref. [14])

6   CONCLUSIONS

This study presented a robust and efficient FE model for the assessment of the failure behavior of HSTCBs of different sizes. Both numerical and experimental benchmarks were used for validating the model accuracy. The comparison with the FE benchmark showed that the detailed modeling of the non-linear interfacial behavior between steel and concrete is not essential for predicting the load-carrying capacity of the beam as well as the overall energy dissipation. Three different sizes of HSTCBs were simulated under three-point loading, showing two principal failure mechanisms, namely the flexural failure at the mid-span and the shear failure along the diagonal direction.

The qualitative analysis of the size and geometrical effects on the load-carrying capacity of the beam showed a combination of the two individual size effects of these failure modes. In particular, for diagonal shear failure, the size effect was described by using the classical Bažant's size effect law of quasibrittle fracture while, in ductile flexural failure, the size effect was derived by a simple plastic analysis. A transition was observed between these two size effects influenced by the 3D geometry of the steel joist and the fracture property of concrete.

It was finally found that a robust computational modeling is required for the design extrapolation of HSTCBs across different sizes and geometries as well as for the analytical modeling of the complete size effect in HSTCBs.

REFERENCES

[1] Tesser, L. and Scotta, S. Flexural and shear capacity of composite steel truss and concrete beams with inferior precast concrete base. *Eng. Struct.* (2013) **49**:135-45.

[2] Campione, G., Colajanni, P. and Monaco, A. Analytical evaluation of steel-concrete composite trussed beam shear capacity. *Materials and Structures* (2016) **49**(8):3159-3176, DOI: 10.1617/s11527-015-0711-6.

[3] Monti, G. and Petrone, F. Shear resisting mechanisms and capacity equations for composite truss beams. *J. Struct. Eng.* (2015) art. no. 04015052, DOI: 10.1061/(ASCE)ST.1943-541X.0001266.

[4] Colajanni, P., La Mendola, L., Latour, M., Monaco, A. and Rizzano, G. Analytical

prediction of the shear connection capacity in precast steel-concrete trussed beams. *Materials and Structures* (2017) **50**(1) art. no. 48, DOI 10.1617/s11527-016-0931-4.

[5] Colajanni, P., La Mendola, L. and Monaco, A. Experimental investigation on the shear response of precast steel-concrete trussed beams. *J. Struct. Eng.* (2016) **43**(1), art. no. 04016156, DOI: 10.1061/(ASCE)ST.1943-541X.0001642, 04016156.

[6] Monaco, A. Numerical prediction of the shear response of semi-prefabricated steel-concrete trussed beams. *Construction and Building Materials* (2016) **124**:462-474, DOI:10.1016/j.conbuildmat.2016.07.126.

[7] Colajanni, P., La Mendola, L. and Monaco, A. Stiffness and strength of composite truss beam to R.C. column connection in MRFs. *J. Constr. Steel Res.* (2015) **113**:86-100, DOI: 10.1016/j.jcsr.2015.06.003.

[8] Tullini, N. and Minghini, F. Nonlinear analysis of composite beams with concrete-encased steel truss. *J. Constr. Steel Res.* (2013) **91**:1-13.

[9] Colajanni, P., La Mendola, L. and Monaco, A. Stress transfer mechanisms investigation in hybrid steel trussed-concrete beams by push-out tests. *J. Constr. Steel Res.* (2014) **95**:56-70.

[10] Colajanni, P., La Mendola, L., Latour, M., Monaco, A. and Rizzano, G. FEM analysis of push-out test response of Hybrid Steel Trussed Concrete Beams (HSTCBs). *J. Constr. Steel Res.* (2015) **111**:88-102, DOI: 10.1016/j.jcsr.2015.04.011.

[11] Bažant, Z. P. and Kazemi, M. T. Brittleness and size effect in concrete structures. *Proc., Engineering Foundation Conference on Advances in Cement Manufacture and Use* (1988), Trout Lodge, Potosi, Missouri, August 1-5, Paper ID n. 5.

[12] Ožbolt., J., Eligehausen, R. and Petrangeli, M. *The size effect in concrete structures*. E&FN Spon., eds., 2-6 Boundary Row, London, ISBN: 0419190406, (1994).

[13] Cedolin, L., and Cusatis, G. Cohesive fracture and size effect in concrete. *Proc., 6th International Conference on Fracture Mechanics of Concrete and Concrete Structures (FraMCOS-6)* (2007), Catania (Italy). June 18-21, 17-29, ISBN 978-0-415-44065-3.

[14] Ballarini, R., La Mendola, L., Le, J. and Monaco, A. A computational study of failure of hybrid steel trussed concrete beams. *J. Struct. Eng.* (2017), **143**(8), art. no. 04017060, DOI: 10.1061/(ASCE)ST.1943-541X.0001792.

[15] Bažant, Z. P. and Yu, Q. Size effect in concrete specimens and structures: New problems and progress. *Proc., 5th International Conference on Fracture Mechanics of Concrete and Concrete Structures (FraMCOS-5)* (2004), Colorado, USA, April 12-16,153-162.

[16] Yu, Q., Le, J.-L., Hubler, M., Wendner, R., Cusatis, G. and Bažant, Z. P., Comparison of main models for size effect on shear strength of reinforced or prestressed concrete beams, *FIB Structural Concrete* (2016), DOI: 10.1002/suco.201500126.

[17] Lee J. and Fenves G.L. Plastic-damage model for cyclic loading of concrete structures. *Journal of Engineering Mechanics* (1998) **124**(8):892–900.

[18] Bažant, Z. P. and Oh, B.-H. Crack band theory for fracture of concrete. *Mater. Struct.* (1983) **16**(3):155–177.

[19] Abaqus 6.12 Theory Manual, Dassault Systèmes Simulia (2012).

[20] Bažant, Z. P. Size effect in blunt fracture: concrete, rock, metal. *J. Eng. Mech.* (1984), **110**(4):518-535.

[21] Bažant, Z. P. Size effect. *International Journal of Solids and Structures* (2000) **37**:69-80.

[22] Bažant, Z.P. *Scaling of Structural Strength*, 2nd Edition, Hermes-Penton Science (2005).